The Reaction of $O_2^+ + C_8H_{10}$ (Ethylbenzene) as a Function of Pressure and Temperature. 2. Analysis of Collisional Energy Transfer of Highly Excited $C_8H_{10}^+$

J. Troe,*,† A. A. Viggiano,‡ and S. Williams‡

Institute for Physical Chemistry, University of Goettingen, Tammannstrasse 6, D-37077 Goettingen, Germany, and Air Force Research Laboratory, Space Vehicles Directorate, 29 Randolph Rd., Hanscom AFB, Massachusetts 01731-3010

Received: September 30, 2003; In Final Form: December 2, 2003

The pressure and temperature dependence of the stabilization vs dissociation yield of chemically activated ethylbenzene ions from the charge-transfer reaction $O_2^+ + C_8H_{10} \rightarrow O_2 + C_8H_{10}^+$ is analyzed. Combining the measured data with experimental specific rate constants, $k(E)$, for dissociation of ethylbenzene ions from the literature allows absolute values of the product $Z\langle\Delta E\rangle$ for energy transfer in the buffer gases He and N_2 to be derived. By assigning the collision frequency Z to the Langevin rate constant, the average energies transferred per collision $\langle\Delta E\rangle$ for highly excited $C_8H_{10}^+$ are obtained. They are close to the corresponding values for neutral alkylbenzenes. $k(E)$ shows a transition from values given by phase space theory at low energies to values arising from an anisotropic valence potential at higher energies. The charge transfer process is analyzed in terms of resonant charge transfer, charge transfer through ethylbenzene$-O_2^+$ complexes, and charge transfer producing electronically excited O_2 molecules, with the former being exploited for the described study of collisional energy transfer.

1. Introduction

Intermolecular collisional energy transfer is a ubiquitous process. It initiates thermal dissociation, terminates the reverse recombination reactions, and deactivates photochemically or chemically activated species. Over the years, much information has been collected on this process in highly excited neutral molecules; see e.g. the reviews in refs 1−5. To date, the most complete information stems from experiments using kinetically controlled selective ionization (KCSI).[6−8] In those experiments both the average energies $\langle\Delta E\rangle$ and average squared energies $\langle\Delta E^2\rangle$ transferred per collision were measured as a function of energy E for a variety of excited molecules and buffer gases M. In addition, collisional transition probabilities $P(E',E)$ from energy E to energy E' could be characterized to some extent. The KCSI results now are not only more detailed than earlier evaluations of pressure-dependent yields in photoactivation and chemical activation experiments (see e.g. refs 1−5 and 9−12), of collision efficiencies β_c in thermal unimolecular reactions (see e.g. refs 13−15), but also of the more direct determinations of $\langle\Delta E\rangle$ such as from hot UV absorption,[16,17] hot IR emission,[18−20] and hot product spectroscopy.[21,22]

Much less information on collisional energy transfer of highly excited molecular ions has been collected, although, in principle, similar techniques to those used for neutral studies can be applied. Some limited information is available from collision efficiencies, β_c, of ion−molecule association reactions in the low-pressure range (see e.g. refs 23−25). Chemical and photochemical activation experiments with a series of buffer gases have been reported for several excited molecular ions.[26−28] Relative collision efficiencies of several bath gases could be derived. Some information on absolute values of collisional deactivation rates has also been obtained; however, the analysis with respect to $\langle\Delta E\rangle$ was either not made or appeared only preliminary. Nevertheless, on the basis of these results, one may conclude that collisional energy transfer from highly excited molecular ions can be characterized by values of $\langle\Delta E\rangle$ which are similar to those observed in the corresponding neutral systems. In contrast, overall capture collision frequencies, Z, for ion−molecule systems are larger than the Lennard-Jones type collision frequencies applying to neutral systems.

In view of the scarcity and indirect character of the data, the present approach intends to provide more information on collisional energy transfer of excited molecular ions by analyzing chemical activation experiments with molecular ions. We take advantage of the turbulent ion flow tube[29−31] which was recently developed in our laboratory. This instrument allows for studies of ion−molecule reactions at pressures up to 1 bar although impurities often limit the maximum value. Temperature dependence studies have been reported up to 573 K, although higher temperatures are now possible. Chemical activation is achieved by charge transfer occurring on resonant and nonresonant pathways and producing highly excited molecular ions. The subsequent fragmentation then is observed in competition to quenching by collisions with the buffer gas. The pressure dependence of the ratio of the parent ion concentration (stabilization) to the fragment ion concentration (dissociation) as a function of pressure provides information on the ratios of the rate constants for collisional stabilization, $\gamma_c Z[M]$, to the energy E-specific rate constants, $k(E)$, for fragmentation of the excited ions. Here γ_c is the chemical activation collision efficiency (to be distinguished from the thermal activation collision efficiency β_c), Z is the total collision frequency, and [M] is the buffer gas concentration. Once $k(E)$ is known from separate absolute rate measurements and Z can be specified, absolute values of γ_c can be derived from the ratio $\gamma_c Z[M]/k(E)$. From these, $\langle\Delta E\rangle$ values follow by solution of a master equation or by equivalent simpler stochastic treatments.[32,33] In

† University of Goettingen.
‡ Air Force Research Laboratory.

10.1021/jp031122r CCC: $27.50
Published on Web 02/05/2004

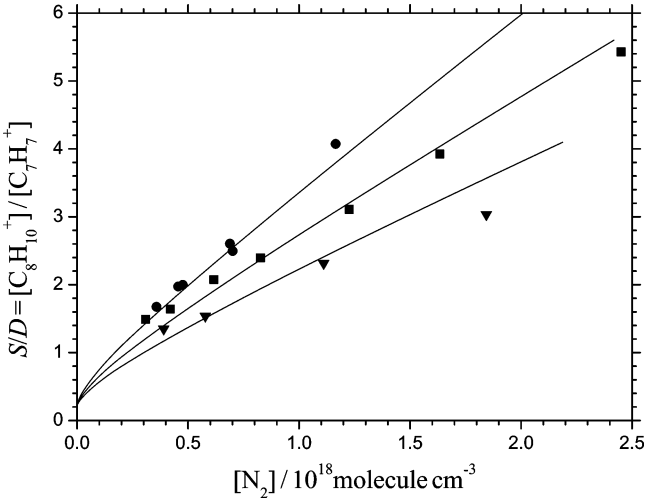

Figure 1. Stabilization vs dissociation yield $S/D = [C_8H_{10}^+]/[C_7H_7^+]$ for the reaction $O_2^+ + C_8H_{10}$ in the buffer gas N_2 (experimental results from ref 31 for 423 (●), 473 (■), and 523 K (▼); full lines = modeling of this work; see section 6).

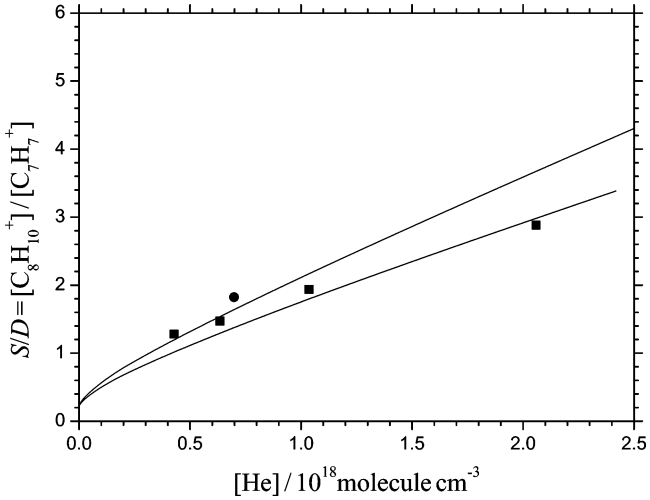

Figure 2. As in Figure 1, for the buffer gas He.

the present work, we analyze experimental results for excited ethylbenzene ions in collisions with M = He and N_2 from ref 31. The present analysis is possible because $k(E)$ has been measured in time-resolved photodissociation experiments[34,35] in a range relevant for our chemical activation experiments. In addition to $k(E)$, also the energy distribution of the excited ethylbenzene ions from the charge transfer process needs to be known. The present work, therefore, provides an analysis of the charge transfer process. To model all the available data, several pathways need to be included, each of which leads to ions with different product ion energy distributions. Studies of energy transfer in highly excited alkylbenzene ions appear particularly attractive, since information on energy transfer in highly excited neutral alkylbenzenes is available from the work discussed in refs 8 and 12. Therefore, a direct comparison of energy transfer data of highly excited neutral and ionic molecules can be made.

2. Experimental Results

Highly excited ethylbenzene ions in ref 31 were produced by charge transfer of C_8H_{10} in collisions with O_2^+ through

$$O_2^+ + C_8H_{10} \rightarrow O_2 + C_8H_{10}^+* \qquad (2.1)$$

Subsequently, the highly excited $C_8H_{10}^+*$ ions were either collisionally stabilized

$$C_8H_{10}^+* + M \rightarrow C_8H_{10}^+ + M \qquad (2.2)$$

or dissociated via

$$C_8H_{10}^+* \rightarrow C_7H_7^+ + CH_3 \qquad (2.3)$$

Minor channels are ignored since they are on the order of impurity ions in the experiment. Relative yields for stabilization vs dissociation, $S/D = [C_8H_{10}^+]/[C_7H_7^+]$, were measured at varying temperatures, T, and concentrations [M] of the buffer gases He and N_2. Details of the measurements have been described in ref 31 and are not repeated here. Figure 1 shows the resulting dependences of S/D on $[N_2]$ for a series of temperatures. Similar experiments with M = He are illustrated in Figure 2. With increasing $[N_2]$ or [He], the yield of stabilized $C_8H_{10}^+$ increases in accordance with the mechanism of reactions 2.2 and 2.3. With decreasing $[N_2]$ or [He], on the other hand, a nonzero intercept of about 0.8 in linear plots of S/D vs [M] is observed. There is no systematic trend in the scatter of the intercepts such that a common intercept tentatively is used for all curves in the analysis.

One could imagine two explanations for the appearance of an intercept in Figures 1 and 2: either the yield curves corresponding to reactions 2.2 and 2.3 at low [M] are nonlinear because of the multistep character of the collisional deactivation process (2.2), or the energy distribution of $C_8H_{10}^+*$ arising from the charge-transfer process (2.1) is so broad that a major fraction of $C_8H_{10}^+*$ is stabilized at much lower pressures than studied here and/or is produced with an internal energy lower than the dissociation limit. Following the analysis of related systems in ref 33, the first possibility can be ruled out such that only the second interpretation can apply. Accepting this, the energy distribution of $C_8H_{10}^+*$ has to be characterized. If reaction 2.1 would proceed via resonant charge transfer,[36] about the difference between the ionization energies of O_2 and C_8H_{10} (12.07 ± 0.008[37] and 8.77 ± 0.01 eV,[34,38] respectively), i.e., E_{ch} = 3.30 eV = 318.3 kJ mol^{-1} = hc 26 608 cm^{-1}, would be transferred to $C_8H_{10}^+$. This is either deposited directly into vibrational energy or into an electronic state that undergoes a rapid intersystem crossing. In either case, the energy is available as vibrational energy on a time scale rapid compared to dissociation.

However, other mechanisms for the charge transfer are possible. Since this is a crucial point to this study, the properties of the charge transfer process (2.1) have to be analyzed more carefully. This analysis is done in section 3. At this stage, we anticipate the result that the rise of S/D with increasing $[N_2]$ in Figure 1 (and with increasing [He] in Figure 2) corresponds to a high-energy fraction of $C_8H_{10}^+*$ originating from resonant charge transfer. At lower pressures, measurements of S/D values smaller than the apparent intercept of Figures 1 and 2 have been made. These include an S/D = 0.33 at 0.2 Torr of N_2 from a selected ion flow tube experiment[31] and S/D = 0.20−0.28 measured in a guided ion beam apparatus under single collision conditions.[39] Accordingly, the complete analysis of the pressure dependence of S/D, from very low to the present high pressures, has to include both dissociations of $C_8H_{10}^+*$ formed at lower energies and those obtained in the resonant process. An analysis of this kind will be given in section 6. It confirms that the low-energy fractions mostly contribute to the apparent intercept of Figures 1 and 2.

TABLE 1: Energy Transfer Properties for Highly Excited Ethylbenzene Ions[a]

	N_2			He	
T/K	423	473	523	423	473
$k(E)/s^{-1}/\gamma_c$	4.8×10^8	6.5×10^8	9.3×10^8	6.6×10^8	9.0×10^8
$I(T)$	0.425	0.348	0.278	0.425	0.348
$\gamma_c(T=0)$	0.124	0.116	0.103	0.095	0.084
$-\langle\Delta E\rangle/cm^{-1}/hc$	269	251	223	206	182
$-\langle\Delta E\rangle/cm^{-1}/hc$		285 ± 150		180 ± 90	

[a] See text; $s^* = 5.824$, $k(E_{ch}) = 2.64 \times 10^7\ s^{-1}$; $E_{ch}/hc = 26\,608\ cm^{-1}$; the upper line of $\langle\Delta E\rangle$ values corresponds to the simplified evaluation described in section 5; the lower line of $\langle\Delta E\rangle$ values are the final optimized result described in section 6.

Separating the low- and high-energy fractions of $C_8H_{10}^{+*}$ in reaction 2.1, the mechanism is

$$O_2^+ + C_8H_{10} \rightarrow O_2 + C_8H_{10}^+ \qquad \alpha k_{cap} \qquad (2.1a)$$

$$O_2^+ + C_8H_{10} \rightarrow O_2 + C_8H_{10}^{+*} \qquad (1-\alpha)k_{cap} \qquad (2.1b)$$

$$C_8H_{10}^{+*} + M \rightarrow C_8H_{10}^+ + M \qquad \gamma_c Z \qquad (2.2)$$

$$C_8H_{10}^{+*} \rightarrow C_7H_7^+ + CH_3 \qquad k(E) \qquad (2.3)$$

It was shown in ref 31 that the overall charge transfer rate constant is independent of pressure (up to 120 Torr) and temperature (up to 573 K) and equal to the Langevin rate constant $k_{cap} = k_L = 2\pi q(\alpha/\mu)^{1/2} \approx 2 \times 10^{-9}\ cm^3\ molecule^{-1}\ s^{-1}$ for capture of O_2^+ and C_8H_{10}. (A minor contribution from the small permanent dipole moment of C_8H_{10}, such as accounted for by the Su−Chesnavich equation, can be neglected.) The $C_7H_7^+$ ion in reaction 2.3 represents both the benzylium and tropylium isomeric ions, and $k(E)$ corresponds to the sum of these two contributions. When $k(E)$ is known from experiments, the analysis of energy transfer rates is not influenced by the partitioning into benzylium and tropylium. However, the interpretation of $k(E)$ nevertheless concerns the question of benzylium vs tropylium formation in the fragmentation of alkylbenzene ions as shown below.

It has been noted before[31] that the slopes of the S/D vs [He] plots are considerably smaller than the corresponding slopes for M = N_2. This is not only due to smaller values of the collision frequencies $Z = k_L$ between $C_8H_{10}^+$ and M but also to smaller values of $\langle\Delta E\rangle$. A quantitative analysis is given below. The marked temperature dependence of the slopes in Figures 1 and 2 is attributed to higher energies of $C_8H_{10}^{+*}$ at higher temperatures since the thermal excitation of C_8H_{10} apparently is carried over into $C_8H_{10}^{+*}$ during resonant charge transfer and can be used for the fragmentation via reaction 2.3.

We represent the yield plots of Figures 1 and 2 by

$$\frac{S}{D} = \frac{[C_8H_{10}^+]}{[C_7H_7^+]} \approx \frac{\alpha}{1-\alpha} + \frac{\gamma_c Z[M]}{(1-\alpha)k(E)} \qquad (2.4)$$

where we identify Z with the Langevin rate constants for $C_8H_{10}^{+*}$ + M collisions. The collisional rates are $k_L \approx 5.4 \times 10^{-10}\ cm^3\ molecule^{-1}\ s^{-1}$ for M = He and $6.6 \times 10^{-10}\ cm^3\ molecule^{-1}\ s^{-1}$ for M = N_2, and we use $\alpha \approx 0.444$, which corresponds to an intercept of 0.8. The resulting values of $k(E)/\gamma_c$ then are summarized in Table 1. It should be emphasized that $k(E)/\gamma_c$ here stands for a suitably averaged value.

The studies from ref 31 also included measurements with M = He and N_2 at 573 K. We did not include these results in our present evaluation because, for the applied conditions, the second term of the right-hand side of eq 2.4 was not large enough to be distinguished from the first term. At these higher temperatures, buffer gas concentrations above about 10^{18} molecules cm^{-3} would have been required to obtain substantial collisional stabilization of $C_8H_{10}^{+*}$. For 573 K, also the onset of thermal dissociation of $C_8H_{10}^+$ contributed to the observations and is not modeled here.

3. Energy Distributions from Charge Transfer

To evaluate the measured $k(E)/\gamma_c$ from section 2 and to extract $\langle\Delta E\rangle$, the energy content of the dissociating $C_8H_{10}^{+*}$ ions has to be known; i.e., the details of the charge-transfer process (2.1) have to be understood. One may think of several pathways for charge transfer, including resonant charge transfer

$$O_2^+ + C_8H_{10} \rightarrow O_2 + C_8H_{10}^{+*}{}_a \qquad (3.1a)$$

charge transfer through intermediate complex formation

$$O_2^+ + C_8H_{10} \rightarrow (O_2 - C_8H_{10})^{+*} \rightarrow O_2 + C_8H_{10}^{+*}{}_b \qquad (3.1b)$$

and charge transfer leading to electronically excited O_2

$$O_2^+ + C_8H_{10} \rightarrow O_2(^1\Delta_g \text{ or } ^1\Sigma_g^+) + C_8H_{10}^{+*}{}_c \qquad (3.1c)$$

It will be shown in section 6 that there is evidence that all three channels occur.

Capture between O_2^+ and C_8H_{10} at long ranges occurs on an ion-induced dipole potential

$$V_i(r) = -\alpha q^2/2r^4 = -C_i/r^4 \qquad (3.2)$$

with $\alpha(C_8H_{10}) = 14.28 \times 10^{-24}\ cm^3$ such that $C_i/hc = 829\,250\ cm^{-1} \times 10^{-32}\ cm^4$. O_2 and $C_8H_{10}^+$ separate on a long-range ion-induced dipole potential $-E_{ch} - C_f/r^4$ which, with $\alpha(O_2) = 1.59 \times 10^{-24}\ cm^3$, leads to $C_f/hc = 92\,330\ cm^{-1} \times 10^{-32}\ cm^4$. The incoming and outgoing potentials interact and allow for the different types of charge transfer. Resonant charge transfer (3.1a) would correspond to an electron jump during the approach of O_2^+ and C_8H_{10} and to a transition to the shallow outgoing potential. This long-range interaction does not allow for energy randomization between O_2 and $C_8H_{10}^+$, and the thermal energies of O_2^+ and C_8H_{10} are mapped into the corresponding distributions of O_2 and $C_8H_{10}^+$ while $E_{ch} = hc\ 26\,608\ cm^{-1}$ would end up as additional vibrational energy of $C_8H_{10}^{+*}{}_a$. Complex-forming charge transfer (3.1b) would correspond to the formation of a $(O_2-C_8H_{10})^{+*}$ complex with stronger interactions, allowing for energy randomization within the complex. This randomization is estimated to happen faster than about 10−100 ps. After randomization, the complex dissociates into $O_2 + C_8H_{10}^{+*}{}_b$, and the energy distribution in $C_8H_{10}^{+*}{}_b$ is characterized by statistical theory. The charge transfer reaction listed in (3.1c) reduces the energy available for $C_8H_{10}^{+*}{}_c$ by the electronic excitation energy of $O_2(^1\Delta_g) = hc\ 7882\ cm^{-1}$ or of $O_2(^1\Sigma_g^+) = hc\ 13\,121\ cm^{-1}$ for a resonant process and potentially more for a complex-forming mechanism. The range of r values corresponding to the interaction of the incoming and outgoing potentials apparently is smaller than that of the centrifugal barriers in the incoming potential which explains why the rate constants for charge transfer coincide with the Langevin expression.[36]

The suggestion of three charge-transfer pathways (3.1a), (3.1b), and (3.1c) is consistent with the experimental observations of S/D in various pressure ranges (see section 6) and

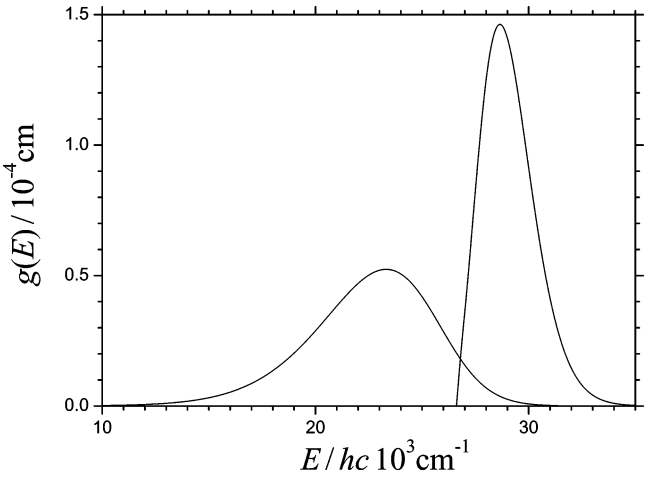

Figure 3. Energy distributions $g(E)$ (in $1/cm^{-1}$) of excited $C_8H_{10}^+$* formed by charge exchange in the reaction $O_2^+ + C_8H_{10}$ ($T = 423$ K, curve at higher energies E: resonant charge transfer with branching ratio 0.45, curve at lower energies E: complex-forming charge transfer with branching ratio 0.367; the curves are normalized with respect to these branching ratios, see text).

follows the results derived for $O_2^+ + C_2H_2$ in ref 40. The direct charge transfer (3.1a), because of the near-resonant $O_2^+ + C_8H_{10}$ and $O_2 + C_8H_{10}^+$ vibrations and suitable Franck−Condon factors, should preferentially lead to near-resonant product state-to-state transitions, superimposed on the vibrational excitation (E_{ch}) in $C_8H_{10}^+$ gained during the electron jump. In this case, the vibrational energy distribution of $C_8H_{10}^+$* should be approximately a Franck−Condon weighted thermal distribution projected at an energy of E_{ch}. The consequences are tested by studying the temperature dependence of S/D. Because the Franck−Condon factors are assumed to be large near resonance, a thermal distribution is used in this study as illustrated in Figure 3. However, it should be emphasized that some distortions of the thermal vibrational distribution because of only near-resonance are possible (see below).

Randomizing E_{ch} in the $(O_2-C_8H_{10})^+$ adduct in reaction 3.1b will lead to statistical energy partitioning between O_2 and $C_8H_{10}^+$. This charge transfer pathway then would lead an energy distribution $P(E,E_{EB})$ in $C_8H_{10}^+$* which is given by

$$P(E,E_{EB}) \approx A\rho_{vib}(E_{EB})W_{rest}(E - E_{EB}) \qquad (3.3)$$

where E_{EB} is the vibrational energy of $C_8H_{10}^+$, ρ_{vib} is the vibrational density of states of $C_8H_{10}^+$, W_{rest} is the number of states of the internal degrees of freedom of the dissociating $(O_2-C_8H_{10})^+$ adduct excluding the vibrations of $C_8H_{10}^+$, E is the total energy available for partitioning at sufficiently large $(O_2-C_8H_{10})^+$ distances, and A is a normalization factor such that $\int_0^E P(E,E_{EB})\, dE_{EB} = 1$. We have characterized W_{rest} either by the O_2 vibration, relative translation, and rotations of O_2 and $C_8H_{10}^+$ or by O_2 vibration and low-frequency deformation vibrations of the $(O_2-C_8H_{10})^+$ complex. $\rho_{vib}(E_{EB})$ was determined by accurate state counting with the frequencies given in ref 34. The resulting broad energy distributions in $C_8H_{10}^+$* look quite similar to those for C_6H_6 from the dissociation $C_8H_8 \rightarrow C_6H_6 + C_2H_2$ in Figure 9.4 of ref 41. $P(E,E_B)$ can well be approximated by an analytical expression

$$P(E,E_B) \approx A'(E - E_B)^5 \exp[-5(E - E_B)/(E - E_B)_{max}] \quad (3.4)$$

where $(E - E_B)_{max}$ corresponds to the energy of the maximum of the distribution. For a translational/rotational model of $(O_2-C_8H_{10})^+$ and $E/hc \approx 31\,000$ cm^{-1} (i.e., $E \approx E_{ch} + E_{th}(432\text{ K})$), we derived $(E - E_B)_{max}/hc \approx 3800$ cm^{-1}; for a low-frequency vibrational model of $(O_2-C_8H_{10})^+$, we calculated $(E - E_B)_{max}/hc \approx 5500$ cm^{-1}. Apart from the statistical partitioning characterized by eq 3.4, the contribution from thermal excitations of O_2^+ and C_8H_{10} has to be taken into account. To account for the thermal excitation energy E_{th} of C_8H_{10} carried into the complex, which participates in the randomization, the distribution $P(E,E_B)$ finally was convoluted with the thermal distribution of C_8H_{10}. The resulting distribution is included in Figure 3. The energy distributions arising from channel (3.1c) are either of resonant or of complex-forming character. However, the energy available for $C_8H_{10}^+$ is reduced by the electronic excitation energy of O_2 (see section 6).

4. Specific Rate Constants

The S/D results of Figures 1 and 2 correspond to relative rate measurements which lead to absolute rates of collisional energy transfer only when the specific rate constants $k(E)$ can be characterized sufficiently well. It has been demonstrated previously that this approach to energy transfer is viable: in ref 12 vibrationally highly excited neutral alkylcycloheptatrienes and alkylbenzenes were produced via light absorption followed by internal conversion. Stern−Volmer plots for quenching gave ratios $\gamma_c Z[M]/k(E)$ which were found to be fully consistent with separate absolute rate measurements of $\langle\Delta E\rangle Z$ (such as contained in $\gamma_c Z$) and of $k(E)$. The analysis of Figures 1 and 2 closely follows the interpretation of these previous experiments.

The derivation of absolute values of γ_c and of $\langle\Delta E\rangle$ depends on the knowledge of absolute values of the specific rate constants $k(E)$. In the following we rely on the available experimental data for $k(E)$ from refs 34 and 35 and their extension by theoretical work from ref 42. A value for $k(E)$ of $(1.6 \pm 0.4) \times 10^8$ s^{-1} in ref 34 was measured at an energy of 4.02 eV = hc 32 420 cm^{-1} (including a thermal vibrational energy of $C_8H_{10}^+$ of hc 2090 cm^{-1} at 413 K). A range of $k(E)$ were measured in ref 35 between about 2×10^3 s^{-1} at $E/hc =$ 16 200 cm^{-1} and 5×10^6 s^{-1} at $E/hc = 22\,100$ cm^{-1}. The latter results were represented (with an uncertainty of about ±30%) by $k(E) = 1.60 \times 10^8$ s^{-1} [$(E/hc - 14\,843$ cm^{-1})/15 178 cm^{-1}]$^{4.7337}$. We combine the data from refs 34 and 35 into a similar expression

$$k(E) = 1.6 \times 10^8\ \text{s}^{-1}[(E - E_0)/hc\ 18\,350\ \text{cm}^{-1}]^{4.824} \quad (4.1)$$

which will be used in the following. E_0 stands for the dissociation energy of $C_8H_{10}^+$ into benzylium$^+$ + CH_3, which is estimated to be $E_0/hc = 14\,070 \pm 100$ cm^{-1}.[34,38]

The present work corresponds to excitation energies which are in the gap between the experimental conditions of refs 34 and 35. For this reason, the quality of the interpolated $k(E)$ from eq 4.1 has to be verified. This is particularly necessary, as the exponent 4.824 of eq 4.1 appears to be smaller than expected for conventional RRKM calculations like those performed in ref 43. There is the possibility of two $C_7H_7^+$ isomers formed in eq 2.3, namely the benzylium and tropylium ions. These have different threshold energies. Employing the dissociation energy E_0 for formation of benzylium in eq 4.1 does not mean that we assume an exclusive formation of benzylium ions in reaction 2.3. Equation 4.1, at this stage, is only used as an empirical representation of the measured $k(E)$ values. For an interpretation and modeling of $k(E)$ values, however, the branching ratio of the dissociation (2.3) of $C_8H_{10}^+$* into tropylium and benzylium ions should be understood at least semiquantitatively. It is well-

known that the branching ratio should vary with the excitation energy and that the formation of tropylium should be characterized by a barrier for the reverse process while the formation of benzylium does not involve such a barrier.[39,44,45] Without entering into the discussion of the precise value of this branching ratio and its energy dependence,[34,46−48] we realize that the two channels have both to be considered. However, the benzylium channel dominates at the energies of interest to the present work, accounting for greater than 85%[48] of reaction 2.3.

Because any error associated with neglecting this channel is within the error of the calculations, we leave the RRKM modeling of the tropylium channel to ref 48 and here only consider $k(E)$ for the benzylium channel. For this channel, because there is no reverse barrier, $k(E)$ cannot be modeled by conventional, rigid activated complex RRKM theory. Instead, one has to account for the varying character of the potential energy surface of a molecular ion, being of valence type at short interfragment distances similar to neutral molecules, and changing to an electrostatic potential at large interfragment distances. At energies close to threshold, the long-range potential is relevant, which for an isotropic ion-induced dipole potential, such as in the present case, can be treated by phase space theory (PST). In the reverse ion-induced dipole association, this corresponds to a Langevin rate constant.[49] At higher energies, the "effective transition state" of the reaction will move into the range of the valence potential which will reduce $k(E)$ below the values derived from PST. The phenomenon of transition state shifting (or switching) has been known for a long time from adiabatic channel[50,51] or variational transition state treatments.[51−53] A more precise link to the potential energy surface can be established in the statistical adiabatic channel/classical trajectory (SACM/CT) approach of ref 54 which formed the basis of ref 42. The essential part for a calculation of $k(E)$ in any case is the potential. In ref 42 a long-range/short-range switching potential was constructed, employing a recalculated polarizability of CH_3 radicals, being $\alpha(CH_3) = 2.334 \times 10^{-24}$ cm^3 [55] (instead of $\alpha(CH_3) = 9.25 \times 10^{-24}$ cm^3 from ref 34). The polarizability governs the distance at which the potential switches from long range to short range. With this potential, the SACM/CT calculation[42] led to a $k(E,J=0)$ which practically coincides with eq 4.1 after fine-tuning of the calculations to the measured value at 32 420 cm^{-1}. Figure 4 compares eq 4.1 with the measurements. For comparison, $k(E,J=0)$ calculated by PST is also included in Figure 4. As a consequence of the increasing shift of the effective transition state into the more anisotropic short-range part of the potential, $k(E,J=0)$ increasingly drops below the PST result with increasing energy (for more details of the calculation, see ref 42).

The good agreement between measured[34,35] and modeled[42] $k(E)$ provides confidence in the quality of eq 4.1. The accuracy of the measured $k(E)$ is estimated to be about ±30%. One should keep in mind, however, that a J dependence of $k(E,J)$ in the modeling was neglected (see refs 42 and 56). The accuracy of the employed $k(E)$ limits that of the finally derived product $Z\langle\Delta E\rangle$, the uncertainty of $k(E)$ being directly carried over into that of $\langle\Delta E\rangle$.

5. Collision Efficiencies

It will be shown in section 6 that the charge transfer channels (3.1b) and (3.1c) mainly contribute to the apparent intercepts in Figures 1 and 2. The reason is that excited $C_8H_{10}^+$ from these channels (1) to a large extent has been stabilized by collisions in the pressure range of the present experiments or (2) the $C_8H_{10}^+$ is produced with an energy below the dissociation limit.

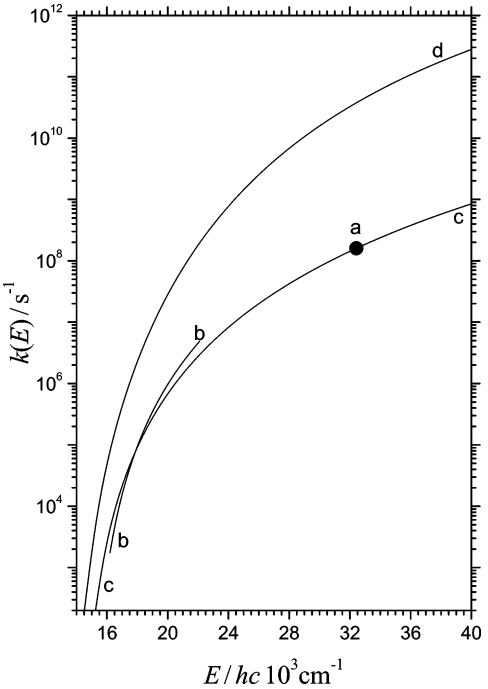

Figure 4. Specific rate constants $k(E)$ for the dissociation $C_8H_{10}^+ \rightarrow C_7H_7^+ + CH_3$ (a, experimental result from ref 34; b, experimental results from ref 35; c, representation of experimental results from refs 34 and 35 by eq 3.1 and by theoretical modeling from ref 42; d, PST modeling of $k(E,J=0)$ for $C_7H_7^+$ = benzylium$^+$, see ref 42).

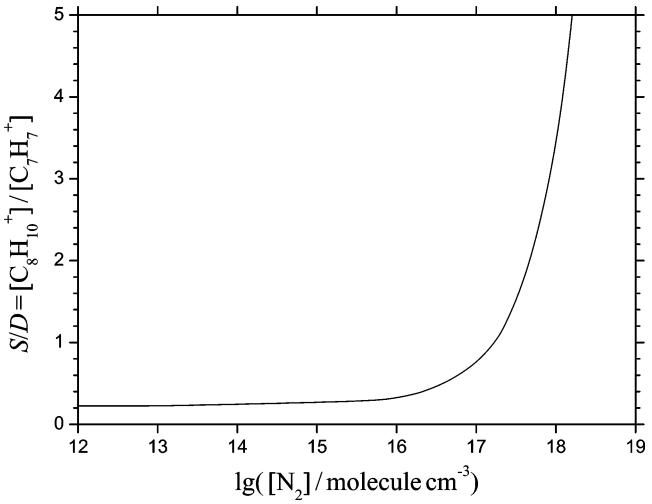

Figure 5. Modeled S/D in the bath gas N_2 at 423 K (see text).

Therefore, we start with the simplified evaluation of our results in terms of eq 2.4. By employing $k(E)$ from eq 4.1, the collision efficiencies γ_c are extracted from the ratios $k(E)/\gamma_c$ given in Table 1. Since not only $k(E)$ but also γ_c depends on the energy E, eq 2.4 implies averaging of the ratio $\gamma_c(E)/k(E)$ over the energy distribution from channel (3.1a) which, according to section 3, should be close to thermal. Taking into account that the fraction α only very weakly depends on the excitation energy (see section 3) and that the energy E is given by the sum of the exothermicity, E_{ch}, of the charge transfer process (2.1), i.e., 3.30 eV = hc 26 608 cm^{-1} (see section 2), and the thermal vibrational energy of C_8H_{10} transferred into $C_8H_{10}^+$*, eq 2.4 reads

$$\frac{S}{D} = \frac{\alpha}{1-\alpha} + \frac{Z[\mathrm{M}]}{1-\alpha}\int_{E_{ch}}^{\infty} f(E,T)\frac{\gamma_c(E)}{k(E)}\,\mathrm{d}E \qquad (5.1)$$

where $f(E,T)$ corresponds to the thermal vibrational distribution

of C_8H_{10}. The justification for using a linear dependence of S/D on the buffer concentration [M], for each slice dE of the energy distribution $f(E,T)$, comes from the solution of the master equation for competing dissociation of $C_8H_{10}^+$* and collisional energy transfer, such as discussed in ref 33. The master equation has the form

$$dn(E,J,t)/dt = -\{Z[M] + k(E,J)\}n(E,J,t) + Z[M]\int_0^\infty dE' \int_0^\infty dJ' P(E,J;E',J') n(E',J',t) \quad (5.2)$$

where $P(E,J;E',J')$ is the collisional transition probability from (E',J') to (E,J) and $n(E,J,t)$ is the level population. Neglecting the J dependence, eq 5.2 in ref 33 was solved for reactions with similar properties as the present system. It was found that, except for very small [M], a linear relationship like eq 5.1 is approached. Furthermore, except for E very close to the dissociation threshold energy E_0 of $C_8H_{10}^+$, the solution of the master equation coincides with that of a much simpler stochastic model. If $k(E)$ can be represented in the form

$$k(E) \propto (E - E_0)^{s^*-1} \quad (5.3)$$

and E_{ac} denotes the initial excitation energy, then the collision efficiency γ_c is well approximated by[33] (see also ref 57)

$$\frac{\gamma_c}{1-\gamma_c^{\,n}} \approx \frac{-\langle\Delta E\rangle s^*}{E_{ac} - E_0} \quad (5.4)$$

with $n \approx 2$ (n has to be modified if $E_{ac} \rightarrow E_0$[33,58]). Since $k(E)$ from eq 4.1 is of the form of eq 5.3, eq 5.4 serves our purpose, providing a direct access from γ_c to $\langle\Delta E\rangle$.

At γ_c markedly smaller than unity, which is the case here, the term $\gamma_c^{\,n}$ in the denominator of eq 5.4 can be neglected. Equations 4.1, 5.1, and 5.4 then can be combined into

$$\frac{S}{D} \approx \frac{\alpha}{1-\alpha} + \frac{Z[M](-\langle\Delta E\rangle)s^*}{(1-\alpha)k(E_{ch})(E_{ch} - E_0)} I(T) \quad (5.5)$$

where

$$I(T) = \int_0^\infty \left(\frac{E_{ch} - E_0}{E_{ch} - E_0 + E_{th}}\right)^{s^*} \left(\frac{E_{th} + E_{ch}}{E_{ch}}\right) \frac{\rho(E_{th})}{Q_{vib}} \times \exp\left(-\frac{E_{th}}{kT}\right) dE_{th} \quad (5.6)$$

(we here assume that $\langle\Delta E\rangle$ is nearly temperature independent[17] and is roughly proportional[8] to E). Table 1 includes our calculated values for $I(T)$, $\gamma_c(T=0)$ as defined by $\gamma_c(T=0) = (-\langle\Delta E\rangle)s^*/(E_{ch} - E_0)$ and being the apparent collision efficiency at 0 K (under the condition that $\langle\Delta E\rangle$ is temperature independent), and the finally resulting $\langle\Delta E\rangle$.

6. Contributions from Nonresonant Charge Transfer

Experimental evidence for a contribution from heretofore neglected charge transfer pathways (3.1b) and (3.1c) comes from the S/D values measured in the 0.1−1 Torr range[31,39,46] and under single collision conditions in refs 39 and 59. We first consider single collision experiments. At 10^{-8} Torr and 294 K, $S/D = 0.22$ was measured in ref 59 after an observation time of 1 s, whereas $S/D = 0.28$ was obtained in[39] at 2×10^{-4} Torr, 300 K, and an observation time of about 10^{-4} s. Evaluating the properties of the pathways (3.1a) and (3.1b) with respect to energy distributions and the corresponding $k(E)$ clearly indicates that the single collision values of S/D must originate from pathways such as (3.1c) which generate $C_8H_{10}^+$* with very low energy. Either $C_8H_{10}^+$* from this pathway is nondissociative from the beginning, or it is stabilized by radiative cooling on a 10^2 s^{-1} time scale. For this reason, $S/D = 0.22$ is taken as the contribution from channel (3.1c). We use g_i to represent the branching fraction in reaction 3 for channel i. Converting S/D into branching fraction, we find $g_c = 0.180$ ($= S/(S + D)$) as long as the other channels do not contribute to S at the lowest applied low pressure. The contribution from channel (3.1b) (see below) raises g from 0.180 to 0.183. Minor changes of this value have only negligible influence on our later analysis.

The partitioning of the charge transfer between the channels (3.1a) and (3.1b) is more difficult to analyze. It could be done uniquely if S/D were measured over a very broad pressure range. In the present case, only fragmentary information is available for intermediate pressures. S/D values in the bath gas helium of 0.28 at 500 K and about 0.4 Torr (SIFT) and of 0.25−0.28 at 500 K, 0.20 at 600 K, 0.17 at 700 K, and about 1 Torr (HTFA) were reported in ref 39. For 0.2 Torr of N_2 at 473 K, $S/D \approx 0.33$ was measured.[31] In comparison to the measured $S/D = 0.22-0.28$ at $10^{-4}-10^{-8}$ Torr (see above), these values appear too large to be accounted for by channels (3.1a) and (3.1c) alone (see below). Thus, a contribution from channel (3.1b) with the energy distribution from eqs 3.3 and 3.4 must also be present. The α value derived in section 2, at first sight, would correspond to a branching fraction into channel (3.1a) of $g_a = (1 - \alpha) = 0.556$ (from $\alpha = 0.444$, see section 2). As a consequence, a branching fraction of $g_b = 1 - g_a - g_c = 0.261$ would remain for channel (3.1b). On the basis of this partitioning, we modeled the S/D values analogous to section 5 through

$$\frac{S}{D} = Z[M]\int_0^\infty g(E,T)\gamma_c(E)/k(E)\, dE \quad (6.1)$$

where $g(E,T)$ denotes the combined energy distribution of $C_8H_{10}^+$*, generated by channels (3.1a), (3.1b), and (3.1c) with the branching fractions $g_a = 0.556$, $g_b = 0.261$, and $g_c = 0.183$, respectively, and where $\gamma_c(E)$ was based on the $\langle\Delta E\rangle$ values from the evaluation described in section 5 (see Table 1). The resulting S/D were about a factor of 1.5 smaller than shown in Figures 1 and 2. The reason is easily understood: the energy distributions of channels (3.1a) and (3.1b) overlap, and part of the distribution from channel (3.1b) reaches into the range of channel (3.1a) (see Figure 3) and, therefore, should be included in the factor $1 - \alpha$ in eq 5.1. For this reason, the branching fraction for channel (3.1a) $g_a = 0.556$ and the values for $\langle\Delta E\rangle$ have to be modified.

Unfortunately, g_a and $\langle\Delta E\rangle$ cannot be fitted independently when experiments in a limited pressure range are available. For this reason, Figures 1 and 2 alone do not provide unique solutions for g_a and $\langle\Delta E\rangle$. For instance, considering the extreme cases $g_a = 0$ or $g_a = 1 - g_c = 0.817$, Figure 1 ($M = N_2$) would be reproduced within the experimental scatter with $-\langle\Delta E\rangle/hc \approx 50$ cm^{-1} (for $(E - E_B)_{max}/hc = 5500$ cm^{-1} in eq 3.4) and 100 cm^{-1} (for $(E - E_B)_{max}/hc = 3800$ cm^{-1}), or $-\langle\Delta E\rangle/hc \approx 500$ cm^{-1}, respectively. However, for $T = 473$ K and 0.2 Torr, this would give $S/D = 0.26$ and 0.30, or 0.23, respectively. This is smaller than the experimental S/D of 0.33. Also, in the extreme cases $g_a = 0$ and $g_a = 0.817$, neither T nor P dependences of S/D are well reproduced over the full range of Figure 1. Similar discrepancies are observed for the He data of Figure 2. Having fixed the worst case uncertainties of $\langle\Delta E\rangle$, for $M = N_2$ being 50 cm^{-1} < $-\langle\Delta E\rangle/hc$ < 500 cm^{-1}, we

optimized the fit to all of the data, taking into account that the branching rations g_a, g_b, and g_c are independent of the buffer gas M.

Including the measured *S*/*D* values in the pressure range 0.1−1 Torr for M = N_2 and He reduces the uncertainty in the fitting of *S*/*D*. For example, taking $(E - E_b)_{max}/hc = 3800$ cm^{-1} in eq 3.4 (i.e., a statistical energy distribution with a translational/rotational $(O_2-C_8H_{10})^+$ model), $g_a = 0.45$, $g_b = 0.367$, and $g_c = 0.183$, one finds $-\langle\Delta E\rangle/hc = 320$ cm^{-1} for M = N_2 and 210 cm^{-1} for M = He. These values reproduce the data well as shown by the lines in Figures 1 and 2. In addition, the *S*/*D* values of 0.26 for 0.2 Torr of N_2 at 473 K and 0.31 at 1 Torr of He at 473 K were fitted within ±20% of the experiments. If $(E - E_B)_{max}/hc = 5500$ cm^{-1} in eq 3.4 (i.e., a low-frequency vibrational model for $(O_2-C_8H_{10})^+$) is chosen, the best fit finds $-\langle\Delta E\rangle/hc \approx 250$ cm^{-1} for M = N_2 and ≈150 cm^{-1} for He. Our final results for $-\langle\Delta E\rangle/hc$, therefore, are 285 ± 150 cm^{-1} for M = N_2 and 180 ± 90 cm^{-1} for M = He where the estimated uncertainty includes the contributions from the measurements, the fit, and the input values for $k(E)$.

7. Properties of Energy Transfer

The derived average energies transferred per collision, $\langle\Delta E\rangle$, are of similar magnitude as the corresponding values for excited neutral molecules of comparable size; e.g., $-\langle\Delta E\rangle/hc \approx 100$ cm^{-1} for M = He and ≈ 200 cm^{-1} for M = N_2 were obtained[8] for excited neutral toluene at an excitation energy of $E/hc =$ 26 700 cm^{-1}, which corresponds to the present excitation energy E_{ch}. $\langle\Delta E\rangle$ values for M = N_2, also at excited temperatures, were found to be about twice as large as for M = He in excited neutral toluene.[17] The main differences in the energy transfer properties of highly excited neutral and ionic polyatomic molecules, thus, are not in the $\langle\Delta E\rangle$ values but in the overall collision frequencies Z. Experiments of the present type are only sensitive to the product $Z\langle\Delta E\rangle$. The present evaluation, therefore, is consistent with identification of Z as the capture rate constant, i.e., the Langevin rate constant for the $C_8H_{10}^+$−He (or N_2) collisions, and with $\langle\Delta E\rangle$ values such as known from neutral excited molecules. Nevertheless, one should keep in mind that because of the uncertainties in the energy distributions of $C_8H_{10}^+$* generated by several charge-transfer pathways, the derived $\langle\Delta E\rangle$ values also have a considerable uncertainty.

Earlier studies on collisional energy transfer of excited ions from refs 26 and 27 appear in line with the present data. Although these measurements could not directly be evaluated with respect to the absolute value of the product $Z\langle\Delta E\rangle$, at least ratios of $\langle\Delta E\rangle$ for M = He and N_2 could be extracted after accounting for the relevant collision frequencies *Z*. The values of $\langle\Delta E\rangle_{M=He}$:$\langle\Delta E\rangle_{M=N_2} = 0.58$ for excited $C_5H_9^+$ from ref 26 and of 0.47 for excited $C_6H_5Br^+$ from ref 27 are only slightly lower than the present ratio of about 0.6. The similarity of $\langle\Delta E\rangle$ values for excited ions and excited neutrals does not appear unreasonable. Under the present conditions $\langle\Delta E\rangle$ is governed by short-range interactions between the excited species and M, and these should not be characteristically different in ions and neutrals.

8. Conclusions

The present study demonstrates that our turbulent ion flow tube allows for the quantitative investigation of relative efficiencies for collisional stabilization vs dissociation of highly vibrationally excited polyatomic molecular ions. Once the dissociation rates are known from separate time-resolved measurements, absolute values for the product $Z\langle\Delta E\rangle$ can be obtained. Assuming that *Z* is given by the ion-buffer gas capture rate constant (in the present case the Langevin rate constant), $\langle\Delta E\rangle$ values for $C_8H_{10}^+$* collisions with He or N_2 were derived. The values are similar in magnitude to the corresponding values for excited neutral alkylbenzenes. The temperature dependences of the relative stabilization efficiencies could be accounted for within the uncertainties of the energy dependence of the dissociation rates. More detailed measurements of the dissociation rates appear desirable to provide a more reliable evaluation of the present relative efficiency measurements. Likewise, a better understanding of the properties of charge transfer processes generating the vibrationally excited molecular ions is necessary to reduce the error. To some extent, such information can come from detailed measurements of relative efficiencies for collisional stabilization vs dissociation with a variation of the buffer gas pressure over wider ranges than possible in the present work.

Acknowledgment. We are grateful to K.-M. Weitzel for providing and discussing his results[35] prior to publication. In addition, discussions with R. Dressler on charge transfer mechanisms and T. M. Fridgen on single collision results were most helpful. Finally, ab initio calculations of polarizabilities by P. Botschwina[55] are acknowledged. This project was funded by the United States Air Force Office of Scientific Research under Project 2303EP4 and Grant Award F49620-03-1-0012. Financial support by the Deutsche Forschungsgemeinschaft (SFB 357 "Molekulare Mechanismen unimolekularer Reaktionen") is also acknowledged.

References and Notes

(1) Tardy, D. C.; Rabinovitch, B. S. *Chem. Rev.* **1977**, *77*, 373.

(2) Quack, M.; Troe, J. In *Gas Kinetics and Energy Transfer;* Ashmore, P. G., Donovan, R. J., Eds.; The Chemical Society: London, 1977; Vol. 2, p 175; *Int. Rev. Phys. Chem.* **1981**, *1*, 97.

(3) Hippler, H.; Troe, J. In *Gas-Phase Bimolecular Processes*; Baggott, J. E., Ashfold, M. N., Eds.; The Chemical Society: London, 1988; p 209.

(4) Oref, I.; Tardy, D. C. *Chem. Rev.* **1990**, *90*, 1407.

(5) Flynn, G. W.; Parmenter, C. S.; Wodtke, A. M. *J. Phys. Chem.* **1996**, *100*, 12817.

(6) Luther, K.; Reihs, K. *Ber. Bunsen-Ges. Phys. Chem.* **1988**, *92*, 442.

(7) Hold, U.; Lenzer, Th.; Luther, K.; Reihs, K.; Symonds, A. C. *Ber. Bunsen-Ges. Phys. Chem.* **1977**, *101*, 552; *J. Chem. Phys.* **2000**, *112*, 4076.

(8) Lenzer, Th.; Luther, K.; Reihs, K.; Symonds, A. C. *J. Chem. Phys.* **2000**, *112*, 4090. Grigoleit, U.; Lenzer, Th.; Luther, K.; Mützel, M.; Takahara, A. *Phys. Chem. Chem. Phys.* **2001**, *3*, 2191.

(9) Georgakos, J. H.; Rabinovitch, B. S. *J. Phys. Chem.* **1972**, *56*, 5921 (and earlier references cited).

(10) Marcoux, P. J.; Siefert, E. E.; Setser, D. W. *Int. J. Chem. Kinet.* **1975**, *7*, 473 (and earlier references cited).

(11) Orchard, S. W.; Thrush, B. A. *Proc. R. Soc. London* **1972**, *A329*, 233 (and earlier references cited).

(12) Luu, S. H.; Troe, J. *Ber. Bunsen-Ges. Phys. Chem.* **1973.** *77*, 325. Troe, J.; Wieters, W. *J. Chem. Phys.* **1979**, *71*, 3931. Hippler, H.; Troe, J.; Wendelken, H. J. *J. Chem. Phys.* **1983**, *78*, 6709, 6718. Hippler, H.; Luther, K.; Troe, J.; Wendelken, H. J. *J. Chem. Phys.* **1983**, *79*, 239.

(13) Chan, S. C.; Rabinovitch, B. S.; Bryant, J. T.; Spicer, L. D.; Fujimoto, T.; Lin, Y. N.; Pavlou, S. P. *J. Phys. Chem.* **1970**, *74*, 13160.

(14) Van den Bergh, H.; Benoit-Guyot, N.; Troe, J. *Int. J. Chem. Kinet.* **1977**, *9*, 223.

(15) Endo, H.; Glaenzer, K.; Troe, J. *J. Phys. Chem.* **1979**, *83*, 2083.

(16) Hippler, H.; Troe, J.; Wendelken, H. J. *Chem. Phys. Lett.* **1981**, *78*, 257; *J. Chem. Phys.* **1983**, *78*, 6709. Damm, M.; Deckert, F.; Hippler, H.; Troe, J. *J. Phys. Chem.* **1991**, *95*, 2005; *Ber. Bunsen-Ges. Phys. Chem.* **1997**, *101*, 1901.

(17) Heymann, M.; Hippler, H.; Troe, J. *J. Chem. Phys.* **1984**, *80*, 1853. Heymann, M.; Hippler, H.; Plach, H. J.; Troe, J. *J. Chem. Phys.* **1987**, 3867.

(18) Rossi, M. J.; Pladziewicz, J. R.; Barker, J. R. *J. Chem. Phys.* **1983**, *78*, 6695. Toselli, B. M.; Brenner, J. D.; Yerram, M. L.; Chin, W. E.; King, K. D.; Barker, J. R. *J. Chem. Phys.* **1991**, *95*, 176.

(19) Hartland, G. V.; Qin, D.; Dai, H. L. *J. Chem. Phys.* **1994**, *101*, 8554; **1995**, *102*, 8557.

(20) Michaels, C. A.; Flynn, G. W. *J. Chem. Phys.* **1997**, *106*, 7055. Michaels, C. A.; Mullin, A. S.; Park, J.; Chou, J. Z.; Flynn, G. W. *J. Chem. Phys.* **1998**, *108*, 2744.
(21) Wall, M. C.; Mullin, A. S. *J. Chem. Phys.* **1998**, *108*, 9658. Wall, M. C.; Lemhoff, A. S.; Mullin, A. C. *J. Phys. Chem. A* **1998**, *102*, 9101.
(22) Wright, S. M. A.; Sims, I. R.; Smith, I. W. M. *J. Phys. Chem. A* **2000**, *104*, 10347.
(23) Viggiano, A. A.; Dale, F.; Paulson, J. F. *J. Geophys. Res.* **1985**, *90*, 7977.
(24) Frost, M. J.; Sharpe, C. R. J. *Phys. Chem. Chem. Phys.* **2001**, *3*, 4536.
(25) Hamon, S.; Speck, T.; Mitchell, J. B. A.; Rowe, B. R.; Troe, J. *J. Chem. Phys.* **2002**, *117*, 2557.
(26) Miasek, P. G.; Harrison, A. G. *J. Am. Chem. Soc.* **1975**, *97*, 714.
(27) Ahmed, M. S.; Dunbar, R. C. *J. Am. Chem. Soc.* **1987**, *109*, 3215 and earlier references.
(28) Barfknecht, A. T.; Brauman, J. I. *J. Chem. Phys.* **1986**, *84*, 3870. Boering, K. A.; Brauman, J. I. *J. Chem. Phys.* **1992**, *97*, 5439.
(29) Arnold, S. T.; Seeley, J. V.; Williamson, J. S.; Mundis, P. L.; Viggiano, A. A. *J. Phys. Chem. A* **2000**, *104*, 5511.
(30) Arnold, S. T.; Viggiano, A. A. *J. Phys. Chem. A* **2001**, *105*, 3527.
(31) Viggiano, A. A.; Miller, T. M.; Williams, S.; Arnold, S. T.; Seeley, J. V.; Friedman, J. F. *J. Phys. Chem. A* **2002**, *106*, 11917 (part 1 of this work).
(32) Kohlmaier, G. H.; Rabinovitch, B. S. *J. Chem. Phys.* **1963**, *38*, 1692; **1963**, *39*, 490.
(33) Troe, J. *J. Phys. Chem.* **1983**, *87*, 1800.
(34) Kim, Y. H.; Choe, J. C.; Kim, M. S. *J. Phys. Chem. A* **2001**, *105*, 5751.
(35) Malow, M.; Penno, M.; Weitzel, K.-M. In *International Gas Kinetics Symposium*, Essen, **2002**; *J. Phys. Chem. A* **2003**, *107*, 10625.
(36) Dressler, R. A.; Levandier, D. J.; Williams, S.; Murad, E. *Comments At. Mol. Phys.* **1998**, *34*, 43.
(37) Chase, M. W. *NIST-JANAF Thermochemical Tables*, 4th ed.; *J. Phys. Chem. Ref. Data Monogr.* **1998**, *No. 9*.
(38) Lias, S. G.; Bartmess, J. E.; Liebman, J. F.; Holmes, J. L.; Levine, R. D.; Mallard, W. G. *J. Phys. Chem. Ref. Data* **1988**, *17* (Suppl. 1).
(39) Williams, S.; Midey, A. J.; Arnold, S. T.; Morris, R. A.; Viggiano, A. A.; Chiu, Y.-H.; Levandier, D. J.; Dressler, R. A.; Berman, M. R. *J. Phys. Chem. A* **2000**, *104*, 10336.
(40) Chiu, Y.-H.; Dressler, R. A.; Levandier, D. J.; Williams, S.; Murad, E. *J. Chem. Phys.* **1999**, *110*, 4291.
(41) Baer, T.; Hase, W. L. *Unimolecular Reaction Dynamics. Theory and Experiments;* Oxford University Press: Oxford, 1996.
(42) Troe, J.; Ushakov, V. G.; Viggiano, A. A.; Williams, S. *J. Chem. Phys.*, to be submitted.
(43) Hwang, W. G.; Moon, J. H.; Choe, J. C.; Kim, M. S. *J. Phys. Chem. A* **1998**, *102*, 7512.
(44) Buschek, J. M.; Ridal, J. J.; Holmes, J. L. *Org. Mass Spectrom.* **1988**, *23*, 543.
(45) Grotemeyer, J.; Gruetzmacher, H.-F. *Org. Mass Spectrom.* **1982**, *17*, 353. Lifshitz, C. *Acc. Chem. Res.* **1994**, *27*, 138.
(46) Arnold, S. T.; Dotan, I.; Williams, S.; Viggiano, A. A.; Morris, R. A. *J. Phys. Chem. A* **2000**, *104*, 928.
(47) Jackson, J. A.; Lias, S. G.; Ausloos, P. *J. Am. Chem. Soc.* **1977**, *99*, 7515. Dunbar, R. C. *J. Am. Chem. Soc.* **1975**, *97*, 1382.
(48) Fridgen, T. D.; McMahon, T. B.; Troe, J.; Viggiano, A. A.; Midey, A. J.; Williams, S. *J. Phys. Chem. A*, submitted.
(49) Troe, J. *Chem. Phys. Lett.* **1985**, *122*, 425.
(50) Gaedtke, H.; Troe, J. *Ber. Bunsen-Ges. Phys. Chem.* **1973**, *77*, 24.
(51) Quack, M.; Troe, J. *Ber. Bunsen-Ges. Phys. Chem.* **1974**, *78*, 240; **1977**, *81*, 329.
(52) Chesnavich, W. J.; Bass, L.; Su, T.; Bowers, M. T. *J. Chem. Phys.* **1981**, *74*, 2228. Song, K.; Chesnavich, W. J. *J. Chem. Phys.* **1989**, *91*, 4664.
(53) Wardlaw, D. M.; Marcus, R. A. *J. Chem. Phys.* **1985**, *83*, 3462. Hase, W. L.; Duchovic, R J. *J. Chem. Phys.* **1985**, *83*, 3448. Klippenstein, S. J.; Marcus, R. A. *J. Chem. Phys.***1989**, *91*, 2280.
(54) Maergoiz, A. I.; Nikitin, E. E.; Troe, J.; Ushakov, V. G. *J. Chem. Phys.* **1996**, *105*, 6263, 6270, 6277; **1998**, *108*, 5265, 9987; **2002**, *117*, 4201.
(55) Botschwina, P., private communication, 2003; see ref 42.
(56) Luther, K.; Troe, J.; Weitzel, K. M. *J. Phys. Chem.* **1990**, *94*, 6316.
(57) Snider, N. *J. Phys. Chem.* **1985**, *89*, 1257.
(58) Baggott, J. E.; Law, D. W. *J. Chem. Phys.* **1986**, *85*, 6475.
(59) Fridgen, T. D., private communication, 2003.